## **ARTICLE**

# Elucidating the Origins of Enhanced CO<sub>2</sub> Reduction in Manganese Electrocatalysts Bearing Pendant Hydrogen-Bond Donors

Received 00th January 20xx, Accepted 00th January 20xx

DOI: 10.1039/x0xx00000x

Steven E. Tignor, a Travis W. Shaw b and Andrew B. Bocarsly \*a

28

Complexes of the general form  $[Mn(X)(CO)_3bpy]$  (X = a variety of monodentate ligands, bpy = 2,2' bipyridine) have been reported to act as electrocatalysts for the reduction of  $CO_2$  to CO. In this work, a series of phenol and anisole substituted bipyridine ligands were synthesized and ligated to a manganese metal center in order to probe for an intramolecular hydrogen-bonding interaction in the transition state of  $CO_2$  reduction. Ligands without the ability to intramolecularly hydrogen bond displayed decreased catalytic current density compared to those with the ability to hydrogen bond with  $CO_2$ . Electrocatalysis was studied by performing voltammetric and bulk electrolysis experiments under argon or  $CO_2$  environments. Measurements of catalytic rates using hydrogen vs. deuterium for the intramolecular H/D-bonding step show that there is an isotope effect associated with the catalysis. The data presented herein suggest a mechanism involving two subsequent equilibrium isotope effects in combination with a primary kinetic isotope effect.

#### Introduction

3

5

6

7

8

9

10

11

12

13

15

16

17

18

19

20

21

23

24

25

Carbon dioxide is an increasingly Earth abundant chemical which has the potential to be used as a feedstock for chemicals and fuels. <sup>1,2</sup> The catalytic reduction of CO<sub>2</sub> has been known for several decades, however it has attracted growing interest in recent years. <sup>3,4</sup> Electrochemical methods are uniquely suited for the catalytic reduction of CO<sub>2</sub> due to the high atom economy associated with these processes. <sup>5</sup> Among these methods transition-metal mediated electrochemical reduction offers the ability to specifically tailor the catalytic active site to better understand the mechanism of CO<sub>2</sub> reduction. <sup>6-10</sup>

One particular type of homogenous transition-metal CO<sub>2</sub> reduction catalyst that is of recent interest is [MnX(CO)<sub>3</sub>(bpy)], where X = Cl<sup>-</sup>, Br<sup>-</sup> or CN<sup>-</sup> and bpy = 2,2'-bipyridine. <sup>11-14</sup> This system has shown the ability to convert CO<sub>2</sub> to CO with high efficiency and excellent selectivity. <sup>15</sup> In addition, this system has advances over the analogous rhenium system in areas such as efficiency and cost. Several groups including ours have examined variations at bpy, such as changing the ligand environment using bulky bipyridine ligands to inhibit dimerization of the catalytically active species for N-heterocyclic carbene (NHC) ligands to modulate the electronics of the complex. <sup>17-20</sup>

Recently, there have been several reports utilizing 50 secondary-coordination sphere activation mode for enhanced catalysis.  $^{21-24}$  In 2015, our group reported a mangane 52

times the catalytic current of the parent complex, [MnBr(CO)<sub>3</sub>bpy]. We suggested that the observed current enhancement might be attributed to intramolecular hydrogen bonding interactions at the CO<sub>2</sub> binding site that are generated by the pendant phenol moiety.

Herein, we present a mechanistic study supporting the viability of this proposal. We show that the catalytic enhancement is highly dependent upon the location of the phenol moiety on the bipyridine ligand, and support the intramolecular hydrogen bonding theory by gathering x-ray

electrocatalyst containing a bipyridine ligand with a phenol

moiety covalently attached to the 6-position on the bpy which

demonstrated enhanced catalytic activity.<sup>25</sup> The performance of this new complex was markedly improved, generating 10.5

Herein, we present a mechanistic study supporting the viability of this proposal. We show that the catalytic enhancement is highly dependent upon the location of the phenol moiety on the bipyridine ligand, and support the intramolecular hydrogen bonding theory by gathering x-ray data to show that the hydrogen to  $CO_2$  distances for the catalytically less active species are beyond the distance of a strong hydrogen bond. Furthermore, complexes without the ability to intramolecularly hydrogen bond ( $\phi$ -OMe instead of  $\phi$ -OH) displayed significant catalytic current decrease when compared to the hydrogen bonding analogues. Finally, an H/D isotope effect study is undertaken to further probe the dynamic role of an intramolecular hydrogen bond in the reduction of  $CO_2$  to CO at a "Mn(CO)3bpy" reaction center.

### **Results and Discussion**

The hydrogen-bonding effect was studied by synthesizing a variety of substituted bipyridine ligands with phenol and anisole at the 4-, 5-, and 6-positions. The product complexes were characterized both spectroscopically (¹H NMR, ¹³C NMR and FTIR) and by single crystal x-ray diffraction. See Figure 1 and Table 1 for the phenolic structural features.

The crystal structures show that the dihedral angle between the phenol and bipyridine ring is influenced by the phenol's

53

<sup>&</sup>lt;sup>a.</sup> Department of Chemistry, Princeton University, Princeton, New Jersey 08544, United States.

b. Address here.

c. Address here.

<sup>†</sup> Footnotes relating to the title and/or authors should appear here.

Electronic Supplementary Information (ESI) available: [details of any supplementary information available should be included here]. See DOI: 10.1039/x0xx00000x

**ARTICLE** Journal Name

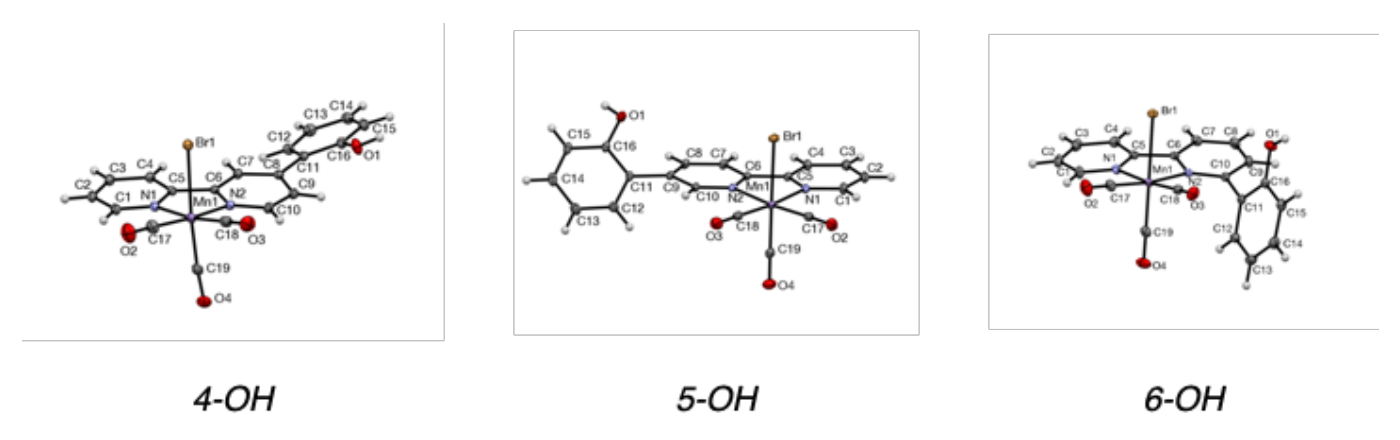


Figure 1. X-ray crystal structures of 4-OH, 5-OH, and 6-OH with ellipsoids set to 50% probability.

position around the ring. In 4-OH this dihedral angle is 24.333 and this increases to 43.40° in 5-OH followed by 64.54° in 6-OB4 The increasing dihedral angle across the complexes is likely d35 to steric repulsion between the pendant phenol group and 36 equatorial CO ligand. Another indication of this steric repulsian is the Mn-N2 (N2 being the nitrogen contained within t88 pyridine ring bearing the substituent phenol) bond length data obtained from the X-ray crystal structures of the three complexes, which shows that this bond length is greatest for 6-OH (Table 1). There is very little variation in the bond length of the Mn-N<sub>1</sub> bond associated with the unsubstituted bipyridine **Table 1.** Dihedral angles, selected bond lengths, and interatomic

| Compound | Dihedral Angle (°) | Mn-N₁ (Å) | Mn-N₂ (Å) | O-Br Interatomic<br>Distance (Å) |
|----------|--------------------|-----------|-----------|----------------------------------|
| 4-OH     | 24.31              | 2.041     | 2.028     | 6.754                            |
| 5-OH     | 43.30              | 2.050     | 2.048     | 6.696                            |
| 6-OH     | 64.54              | 2.035     | 2.091     | 4.425                            |

N1 and N2 are shown in the x-ray structures in Figure 1.

distances for 4-OH, 5-OH, and 6-OH.

12

13

14

15

16

17

18

19

20

21

22

23

24

25

26

27

28

29

30

31

3

4

5

7

8

9

10

The proposed mechanism by which these Mn(I) catalysts are thought to catalyze the reduction of CO<sub>2</sub> to CO is given in Figure 2.26 The primary reduction event is generally accepted to involve addition of an electron to the bpy  $\pi^*$  orbital. This then induces the loss of the axial bromide ligand, opening up a coordination site. A subsequent one electron reduction delivers the active catalyst, which is primed for CO<sub>2</sub> binding. The introduction of a carboxylate ligand is followed by two protonation steps and the loss of a molecule of water. A final electron transfer brings the catalyst back to its active state and yields a molecule of free CO as the reduced product.

The increased dihedral angle for 6-OH compared to 4- and 5-OH is convenient because this places the phenolic OH at a distance from the metal center that is more likely to allow hydrogen bonding to either a bound CO2 or to stabilize the transition state for CO<sub>2</sub> bonding to the metal. In order to further explore the idea that 6-OH can enable a hydrogen bonding interaction by virtue of the distance between the phenolic oxygen to the manganese center while the other isomers cannot, we established the distance between the phenolic oxygen atom and the axial bromide using X-ray crystal structure data (see Figure 3, for example). It is important to note here that we used the bromide precursor as a proxy for the metalcarboxylate species of interest because this adduct is not sufficiently stable to be structurally characterized. This is not surprising given its assignment as a key catalytic intermediate.

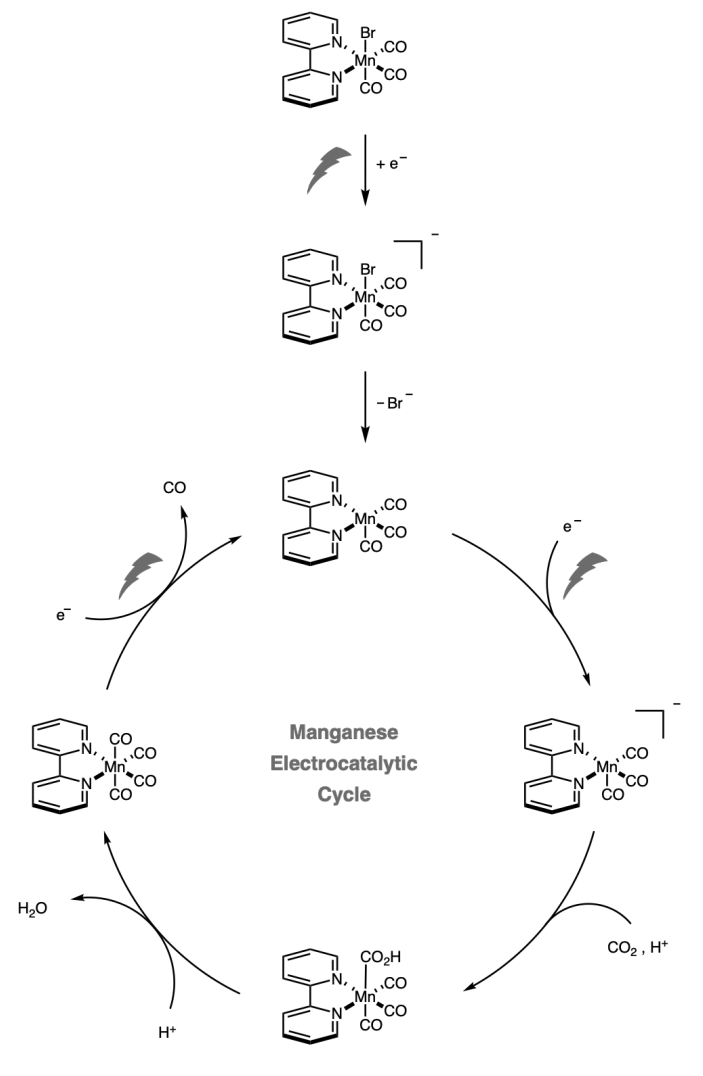


Figure 2. Electrocatalytic cycle for CO<sub>2</sub> reduction mediated by [Mn(bpy)(CO)<sub>3</sub>Br].

Journal Name ARTICLE

1 We assume that the phenolic oxygen-bromide interatom 36 2 distance will accurately reflect the distance between tbd 3 phenolic oxygen atom and the carbon atom of a mangane 38 4 bound CO<sub>2</sub> complex. Under this assumption, the requir 39 5 distance for the hydrogen bond between the phenolic protable 6 and the CO<sub>2</sub> will be approximately equal to the distanted 7 between oxygen and bromine minus an average O-H and C<sub>sp2</sub>42 8 bond length (0.96 Å and 1.2 Å respectively<sup>27</sup>) as shown in Figu#3 9 3. This value corresponds to 2.3 Å for the hydrogen bond in the 10 6-OH, 4.5 Å for the hydrogen bond in the 5-OH, and 4.6 Å f45 11 the hydrogen bond in the 4-OH. Hydrogen bonds with distanc46 12 between 2.4 Å and 2.5 Å fall into the regime of short-stroAd 13 hydrogen bonds as categorized by Anslyn and Dougher4/8 14 meaning that the barrier for the transfer of the hydrogen ato 49 15 between donor and acceptor approaches zero.<sup>28</sup> Furthermor 50 the strength of gas phase hydrogen bonds at a distance of 2.35Å

1.2 Å

1.2 Å

0.96 Å

0.00 H

0.00 H

0.00 CO

0.00

**Figure 3.** Interatomic distances measured from X-ray crystal structure (left). Estimation of distance required for hydrogen bond.

17

18

19

20

21

22

23

24

25

26

27

28

29

30

31

32

33

34

35

is between 30-35 kcal/mol, whereas gas phase hydrogen bonding at a distance of 3.0 Å is only stabilized by  $^{\sim}5$  kcal/mol.  $^{29}$  This rationale suggests that hydrogen-bonding interactions should be more prevalent in 6-OH than in either of the other two isomers.

Additional evidence for the existence of a solution phase steric interaction is found in the <sup>1</sup>H and <sup>13</sup>C NMR spectra of the 6-OH complex. As shown in Figure S4, two sets of peaks indicate that there are two rotameric structures in solution: The phenolic proton exists on either the side of the complex containing the axial bromide ligand, or the side with the axial CO ligand; these two structures do not interconvert on the NMR time scale at 300 K. The 4-OH and 5-OH complexes do not display any such rotameric peaks in their NMR spectra (Figures S10 and S16).

The reduction peak potentials observed by cyclic voltammetry (CV) for the first and second electron reductions are tabulated in Table 2 for the six complexes explored (scan rate data for all complexes and conditions explored are

**Table 2.** 1st and 2nd peak potentials of compounds utilized in this study.

| Compound | 1st Reduction Potential | 2 <sup>nd</sup> Reduction Potential |  |
|----------|-------------------------|-------------------------------------|--|
|          | (V vs. SCE)             | (V vs. SCE)                         |  |
| 4-OH     | -1.15                   | -1.46                               |  |
| 4-OMe    | -1.11                   | -1.43                               |  |
| 5-OH     | -1.14                   | -1.44                               |  |
| 5-OMe    | -1.10                   | -1.40                               |  |
| 6-OH     | -1.14                   | -1.30                               |  |
| 6-OMe    | -1.21                   | -1.30                               |  |

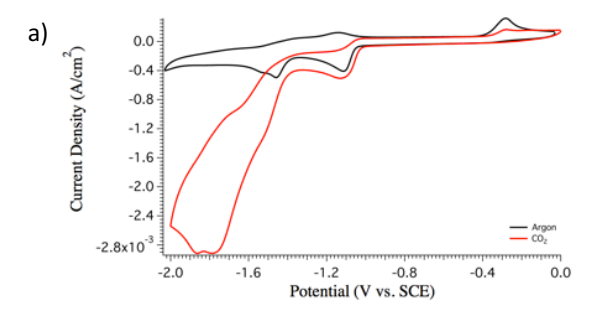
Potentials were measured vs. Ag/Ag\* (0.1 M in MeCN) and were subsequently converted to vs. SCE.

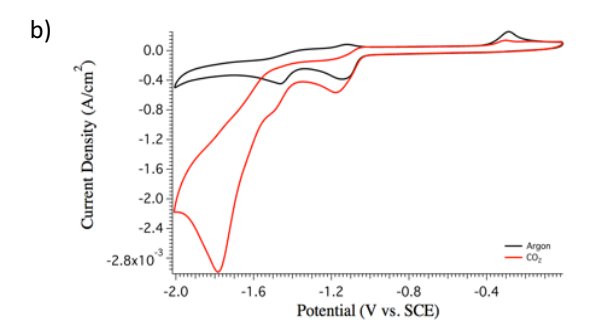
available in Figures S19-S36). The cyclic voltammetry of 4-OH and 5-OH under argon in MeCN with 5%  $H_2O$  each show two reduction peaks at similar potentials (figures S23 and S30; for the CV of 6-OH under the corresponding conditions, see Figure S35).

Overall, the CVs of 4-OH and 5-OH are very similar except for the presence of a small shoulder wave, cathodic to the second reduction wave of 5-OH (see Figure 4). The first-reduction waves for all three phenolic regioisomers are within 10 mV of each other, and the second waves are ~20 mV apart for 4-OH and 5-OH

The second reduction waves for 6-OH and 6-OMe are shifted 140 and 100 mV anodic from 5-OH and 5-OMe, respectively. This could be due to a lack of conjugation between the phenol ring and the bipyridine ring due to a larger dihedral angle between the two rings in 6-OH and 6-OMe, as discussed previously. This would make the phenolic ring a weaker donor in this case, resulting in an anodic shift to the second wave relative to the other, better conjugated, isomers. Ultimately however, changing the connectivity to the bipyridine ring has a minimal effect on the electrochemistry under argon in MeCN with  $5\%~H_2O$ .

The effect of  $CO_2$  on the electrochemistry of 4-OH and 5-OH is much less extreme than for the case of 6-OH (Figure 4). The





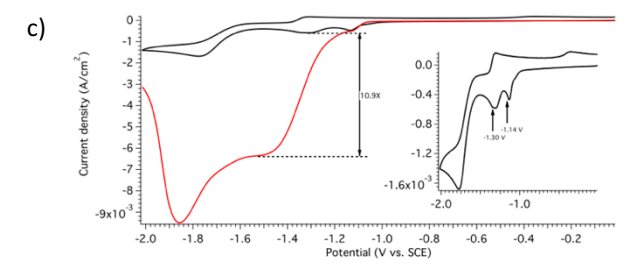


Figure 4. CVs of (a) 4-OH, (b) 5-OH, and (c) 6-OH in MeCN with 5% H<sub>2</sub>O under argon (black) and  $CO_2$  (red) at a scan rate of 100 mV/s.

ARTICLE Journal Name

enhancement at the second reduction wave is only ~2X f34 these two isomers compared to over 10X for 6-OH at 100 mV \$5 In addition, this enhancement is at a greater overpotential th36 with the 6-OH (~500 mV overpotential compared to 400 mV f37 6-OH) causing the catalytic current wave to begin overlappi38 with the third reduction wave. This third reduction wave, whi39 occurs at approximately -1.8 V vs. SCE for all complexes is or40 present under a CO2 atmosphere when protons are included 41 the electrolyte. In controlled potential electrolysis experimen 42 of 6-OH performed in the region of this wave, visible electro 43 fouling was observed, leading us to associate this wave will complex decomposition. One possibility is that this wave corresponds to the reductive decomposition of the manganes 46 carboxylate intermediate.

1

2

3

4

5

6

7

8

9

10

11

12

13

14

15

16

17

18

19

20

21

22

23

24

25

26

27

28

29

31

32

To determine if the phenolic moiety has a role to plane outside of the proposed hydrogen bonding interaction in the 49 OH or 5-OH complexes, we also studied the voltammetry of the methylated complexes, 4-OMe and 5-OMe. Methylation has a very minimal effect on the reduction potentials and overall shape of the voltammograms for both complexes under argon as shown in Table 2 and Figure 5. In MeCN with 5% H<sub>2</sub>O under CO<sub>2</sub>, both complexes show a very similar current enhancement to that of their unmethylated analogs, both increasing by 1.25X (Figure 4). Based on the observation that the methylated analogs are essentially just as active for CO2 reduction as the phenolic systems, we conclude that the phenolic proton plays an insignificant role in the behavior of 4-OH and 5-OH complexes. Notably, this rules out a local proton concentration effect due to the similarities between the -OMe and -OH species of the 4- and 5-substituted complexes.

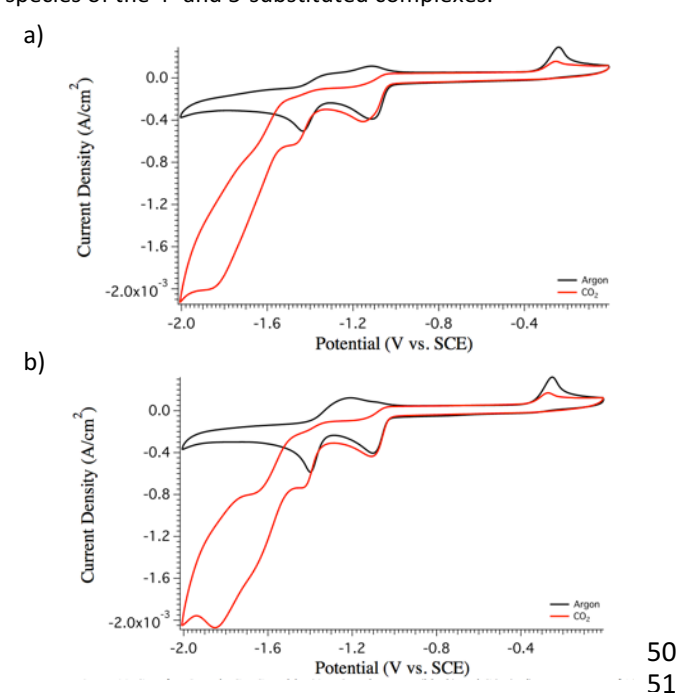
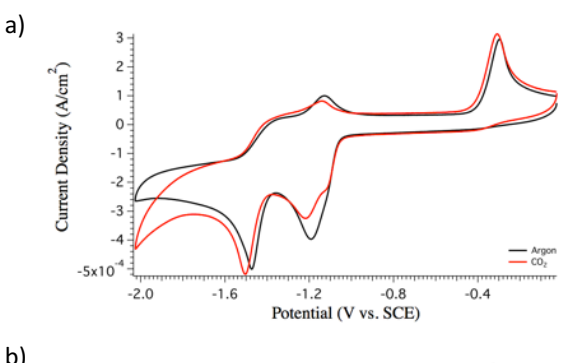


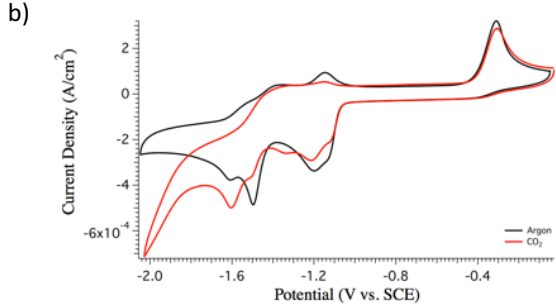
Figure 5. CVs of (a) 4-OMe and (b) 5-OMe with 5% H<sub>2</sub>O under  $argon_2$  (black) and  $CO_2$  (red) at a scan rate of 100 mV/s.

Given that a phenol placed at the 6-position enhances catalytic performance compared to a phenol incorporated the 5- or 4-position, we sought to better understand the

mechanistic underpinnings of this effect. Trivially, protons are required for catalytic conversion of  $CO_2$  to CO; these protons may be for the  $CO_2$  bonding step, or for the C-O bond-breaking step, or for both. The phenolic proton could be enabling  $CO_2$  binding the metal center by forming a hydrogen bond to an incoming  $CO_2$  molecule. This proton-assisted binding would aid in the process of rehybridization, which is one of the barriers in the conversion of  $CO_2$  to CO. Additionally, since the overall chemical process of  $CO_2$  conversion to CO requires two protons and two electrons (forming water in addition to CO), the phenolic proton could be acting as a simple proton donor to facilitate the conversion. To determine if the phenolic moiety could enable C-O bond cleavage, we performed CVs of the complexes in dry MeCN under a  $CO_2$  atmosphere and looked for catalytic current enhancement (Figures 6).

The cyclic voltammetry of 4-OH and 5-OH show no signs of





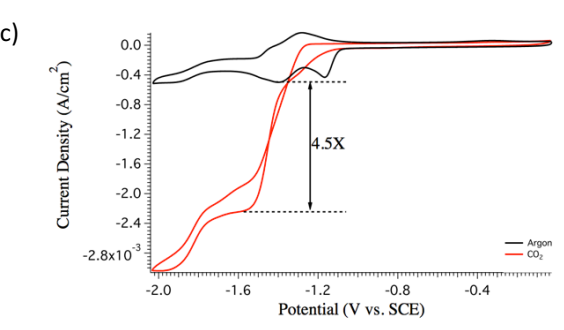


Figure 6. CVs of (a) 4-OH, (b) 5-OH, and (c) 6-OH in dry MeCN under argon (black) and CO2 (red) at a scan rate of 100 mV/s.

catalysis under anhydrous  $CO_2$  (Figure 6a and 6b). The peak shapes for 5-OH are altered in the presence of  $CO_2$ , but no current enhancement can be detected. This may indicate that  $CO_2$  binds to the metal center but no subsequent catalysis occurs. This could signify that the phenol moiety of 5-OH is capable of favoring  $CO_2$  binding, but is not capable of facilitating subsequent catalysis. Voltammetry of the 6-OH isomer is

Journal Name ARTICLE

drastically different under CO<sub>2</sub> than it is under argon in d42 MeCN, as it displays a catalytic current enhancement of 4.543 with an onset at the second reduction wave (Figure 6c) and 44 plateau density, which is indicative of an electrocataly 45 process.

It is possible that in 6-OH the phenol facilitates bonding  $\bf 47$  CO<sub>2</sub> via an intramolecular hydrogen bond, and once bound, t $\bf 48$  phenolic proton can intermolecularly aid in catalytic turnov $\bf 49$  We reason that if appending the phenol at the 6-position aids  $\bf 50$  CO<sub>2</sub> binding *only*, we would see a large effect from adding fr $\bf 54$  phenol when the CV was performed on 6-OH in dry MeCN und  $\bf 52$  a CO<sub>2</sub> atmosphere. If the phenolic moiety helps facilitate C $\bf 53$  bond breaking via a transition state that is dependent on t $\bf 54$  proximity and geometry of the phenol relative to the CO<sub>2</sub> ligan  $\bf 55$  then adding phenol to the electrolyte should have little effec $\bf 56$ 

Figure 7 shows the effect of adding 1, 2, and 10 mM pher to a cell containing 1 mM 6-OH in dry MeCN under CO<sub>2</sub>. No significant current enhancement over the complex alone is observed, even when the proton concentration of the solution is increased by an order of magnitude. This result suggests that the unique position of the phenolic moiety aids in binding and is also important in C-O bond cleavage via an intramolecular pathway.

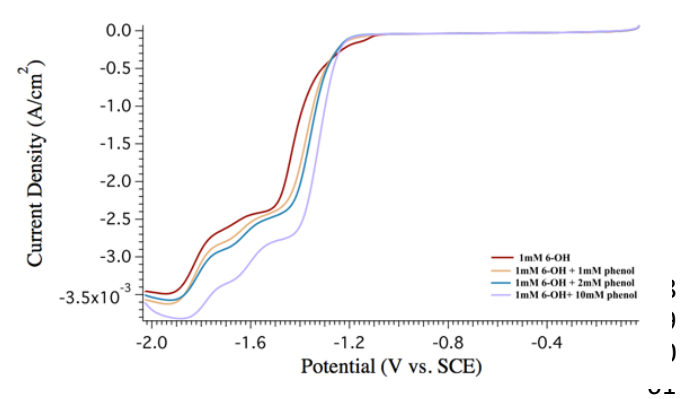


**Figure 7.** Linear sweep voltammetry of 6-OH in dry MeCN under CO<sub>2</sub>! with varying amounts of phenol added to the electrolyte.

The hydrogen-bonding effect associated with the 6-015 complex should be eliminated under wet electrolyte when the 6-OMe complex is used instead. This is what is observed experimentally: the 6-OMe complex displays a significant loss is current enhancement by CV when compared to the 6-OHE complex (Figures S37-S38). Importantly, the 6-OMe complex does display superior current enhancement compared to the parent complex, indicating the location of the substituent is facilitating catalysis, albeit not through an intramolecular hydrogen bond. This result is in agreement with Ngo et. al. and highlights the importance of Lewis basic moieties in close proximity to the open coordination site, thereby switching on what they have referred to as a 'protonation-first' pathway.<sup>24</sup>

#### **Isotope Effect Studies**

To further elucidate the mechanism of catalytic turnover, a series of isotope effect experiments were conducted on the parent complex as well as the 4-OH and the 6-OH complexes.

Experiments using 5%  $H_2O$  and 95% MeCN (v/v) were performed on both complexes, as well as experiments using 5%  $D_2O$  and 95% MeCN. The acidity of phenol assures rapid exchange of the phenol proton with  $H_2O$  (or  $D_2O$ ) in the mixed solvent systems employed. In the presence of 5%  $D_2O$ , there is almost exclusively deutrophenol present when 1mM of Mncomplex is introduced, and thus, this system provides an environment for probing the H/D isotope kinetics exclusively at the phenolic site.

To test the viability of using the described solvent system to probe for an H/D isotope effect a series of cyclic voltammograms using the 6-OH complex were collected under a  $CO_2$  atmosphere with either 5%  $H_2O$  or 5%  $D_2O$  in the electrolyte. Recall that the observed current is a direct measure of the rate of reaction for any reaction sequence that involves one or more charge transfer steps. As shown in Figure 8, there

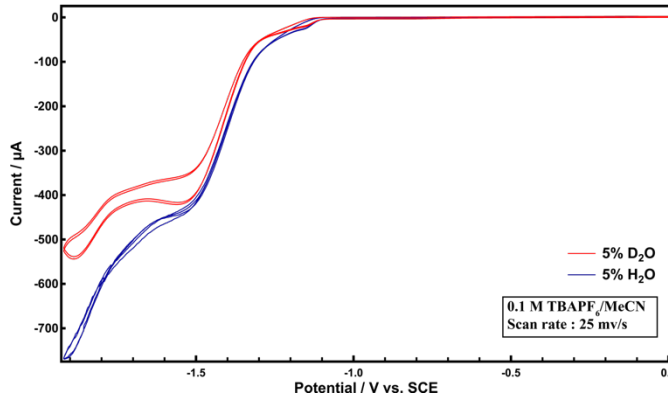


Figure 8. Cyclic voltammetry of the 6-OH complex in either 5%  $H_2O/95\%$  MeCN (blue trace) or 5%  $D_2O/95\%$  MeCN.

is a current enhancement using  $5\%~H_2O$  versus  $5\%~D_2O$  for the 6-OH complex, consistent with an isotope effect. This isotope effect was quantified by doing bulk electrolysis experiments, which gave a direct measurement of the rate of reaction by analyzing CO formation over time. The existence of a rate limiting step during the binding of  $CO_2$  to the metal center would be expected to produce a primary KIE due to the need to break the phenolic O-H bond.

Bulk electrolysis experiments were conducted just past the second CV reduction wave, at -1.72 V vs. SCE using the 5%  $\rm H_2O$  or 5%  $\rm D_2O$  conditions with the parent complex, the 4-OH, and the 6-OH complexes. Samples of the headspace were taken every 20 minutes for 3 hours. The slope of the line of best fit of these time points is a direct measurement of the rate of  $\rm CO_2$  reduction and thus, the ratio of the slopes for a complex under

**Table 3.** Slope of line of best fit for each plot and corresponding isotope effect.

| Compound | Condition           | Slope (µmol<br>CO/min.) | F.E. (%) | Overall Isotope Effect |  |
|----------|---------------------|-------------------------|----------|------------------------|--|
| Parent   | 5% H₂O              | 1.37                    | 76.4     | 1.05                   |  |
| Parent   | 5% D <sub>2</sub> O | 1.34                    | 53.2     |                        |  |
| 4-OH     | 5% H <sub>2</sub> O | 1.89                    | 57.3     | 1.37                   |  |
| 4-OH     | 5% D <sub>2</sub> O | 1.55                    | 54.6     |                        |  |
| 6-OH     | 5% H <sub>2</sub> O | 2.67                    | 77.6     | 1.61                   |  |
| 6-OH     | 5% D <sub>2</sub> O | 1.90                    | 43.8     | 1.01                   |  |

ARTICLE Journal Name

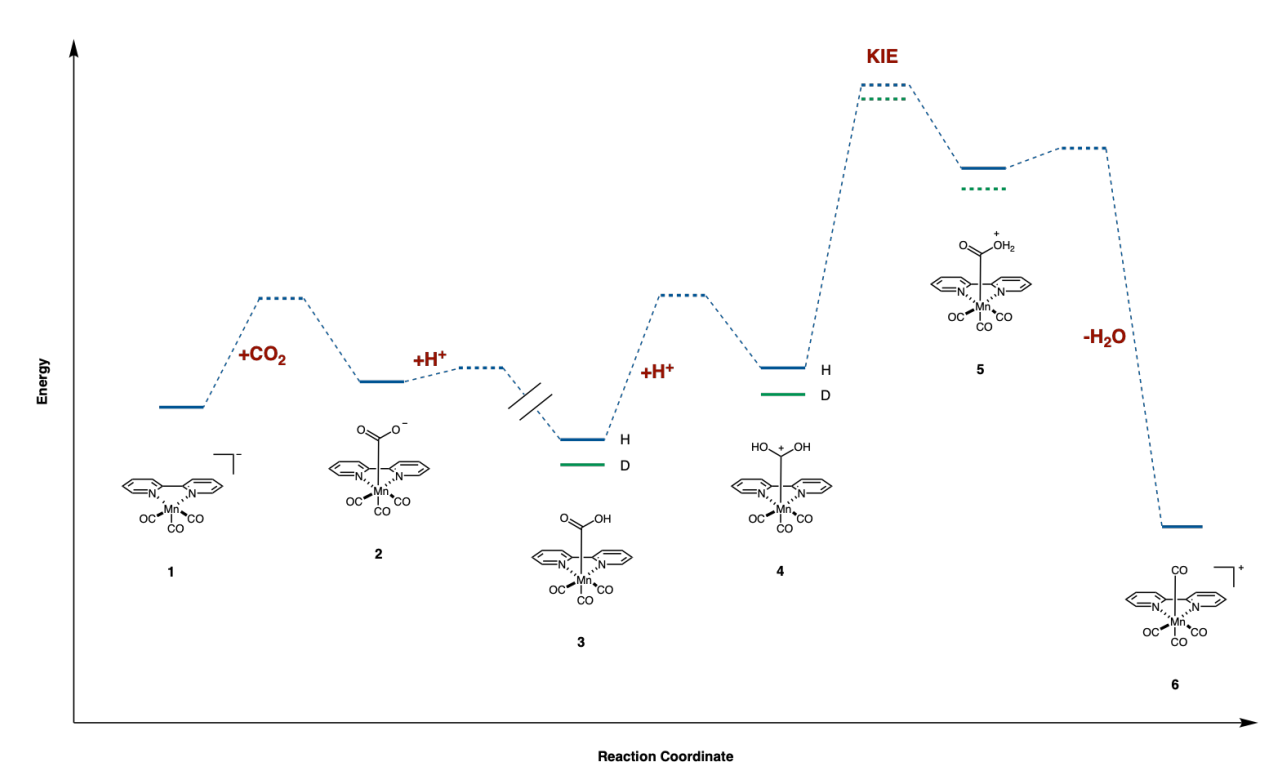


Figure 9. A proposed reaction coordinate diagram which takes into account two equilibrium isotope effects as well as a kinetic isotope effect.  $[\Delta G_{1\rightarrow 2}=+2.2 \text{ kcal/mol}; \Delta G_{1\rightarrow 2}=+3.3 \text{ kcal/mol}; \Delta G_{2\rightarrow 3}=-33.4 \text{ kcal/mol}; \Delta G_{2\rightarrow 3}=-33.4 \text{ kcal/mol}; \Delta G_{3\rightarrow 6}=-27.8 \text{ kcal/mol}; \Delta G_{3\rightarrow 6}=$ 

either the 5%  $H_2O$  or 5%  $D_2O$  conditions is a quantitatised measure of the overall H/D isotope effect. The CO production 2 rates, Faradaic efficiencies, and current vs. time plots a38 provided in Figures S39-S40 and summarized in Table 3 and clearly support the involvement of the phenolic proton due 35the increase in the measured isotope effect from the pare 36 complex to the 4-OH to the 6-OH. Figure 7, which reports tB7 phenol-free control demonstrates that there is a minima8 dependence on the extraneous proton source in solution. Thus 9 the difference in rates of CO production as shown in Figure S\$10 and Table 3 must be coming from the difference between 41 phenolic –OH vs. a phenolic –OD. Furthermore, as the location of the pendant phenolic position becomes more ideal for binding to an incoming CO<sub>2</sub>, the magnitude of the isotope effect? increases accordingly, suggesting this position is crucial for the catalytic rate of these complexes.

There is a clear trend in the isotope effect data in which the greater the ability the complex has to intramolecularly hydrogen bond, the greater the value of the observed overally isotope effect. These data experimentally confirm the prige computational work done by our group as well as that of Carter and Kubiak, where it was proposed that proton-assisted C50 bond cleavage is the rate limiting step. However, pre-equilibrial prior to the rate limiting step occur, each affecting the overally rate through an equilibrium isotope effect. Here, the measures overall isotope effect is an amalgamation of these equilibrium isotope effect for the C-O borgs cleavage event. The magnitude of the overall isotope effecting largest for phenolic moieties positioned optimally for intramolecular hydrogen bonding, and the magnitude

decreases according to the strength of the intramolecular interaction. Based on the results presented by Carter and Kubiak<sup>26</sup>, we propose a mechanism for this overall isotope effect measurement, which is shown in Figure 9. This reaction coordinate diagram utilizes the previous calculation data from Carter and Kubiak to generate the reaction coordinate profile for intermediates 1, 2, 3, and 6. Intermediates 4 and 5 represent likely intermediates in going from complex 3 to complex 6. Notably, this reaction coordinate scheme takes into account the equilibrium isotope effects and subsequent kinetic isotope effect that are in agreement with our experimental rate data.

## **Conclusions**

A series of 2-hydroxyphenyl- and 2-methoxyphenyl-substituted bipyridine ligands were synthesized in order to understand how hydrogen-bond donors in the second coordination sphere affect electrocatalytic CO<sub>2</sub> reduction using a manganese-based electrocatalyst. Voltammetric studies were performed in order to assess the reactivity of the complexes. We observed that significant catalytic current enhancement beyond the unsubstituted bipyridine complex was only realized when the pendant phenol was placed at the 6-position of the bipyridine ligand, the position closest to the ligated metal center. Not only is the phenolic proton's distance minimized when the phenol is at the 6-position, but the torsion angle between the phenol ring and the bipyridine ring may be increased relative to 4- and 5-substituted complexes due to steric interference between the phenol and the manganese center as indicated by X-ray crystal

2

3

4

5

6

7

8

9

10

11

12

13

14

15

16

17

18

20

21

22

23

24

25

27

28

29

Journal Name ARTICLE

1 structures of the complex. The result is a phenolic proton positioned to facilitate binding of a  $CO_2$  ligand and a C-O bon  $\frac{54}{2}$ 2 breaking event of a bound  $CO_2$  ligand. A series of H/D isoto  $\underline{b}\underline{e}$ 3 effect experiments were performed to gain further mechanistic 4 insight. From the data collected there was a clear trend in the 5 value of the observed isotope effect, which correlates well with 6 the complex's ability to intramolecularly hydrogen bo 7 8 affecting both the hypothesized reactive intermediates and the 9 transition state associated with cleavage of the carbon dioxi62 10 C-O bond. 64 65 **Conflicts of interest** 11 66 67 12 There are no conflicts to declare. 68 69 70 **Acknowledgements** 71 Financial support for this work was provided by the National 72 14 Science Foundation under grant CHE-1800400. Any opinions, 7316 findings, and conclusions or recommendations expressed in 75 this material are those of the authors and do not necessarily 17 76 18 reflect the views of the National Science Foundation. 77 78 79 **Notes and references** 19 80 81 20 Whipple, D. T.; Kenis, P. J. A. Prospects of CO2 Utilization via 83 (1) 21 22 Direct Heterogeneous Electrochemical Reduction. J. Phys. 84 23 Chem. Lett. 2010, 1 (24), 3451-3458. 85 24 https://doi.org/10.1021/jz1012627. Rafiee, A.; Rajab Khalilpour, K.; Milani, D.; Panahi, M. Trenda 7 25 (2) 26 in CO<sub>2</sub> Conversion and Utilization: A Review from Process 88 27 Systems Perspective. J. Environ. Chem. Eng. 2018, 6 (5), 89 28 5771-5794. https://doi.org/10.1016/j.jece.2018.08.065. Wang, W.-H.; Himeda, Y.; Muckerman, J. T.; Manbeck, G. F. 91 90 29 (3) Fujita, E. CO<sub>2</sub> Hydrogenation to Formate and Methanol as ag 30 31 Alternative to Photo- and Electrochemical CO<sub>2</sub> Reduction. 93 32 Chem. Rev. 2015, 115 (23), 12936-12973. 94 33 https://doi.org/10.1021/acs.chemrev.5b00197. Jones, J.-P.; Prakash, G. K. S.; Olah, G. A. Electrochemical Co 95 34 (4)35 Reduction: Recent Advances and Current Trends. Isr. J. 97 36 Chem. 2014, 54 (10), 1451-1466. 98 37 https://doi.org/10.1002/ijch.201400081. 99 Bushuyev, O. S.; De Luna, P.; Dinh, C. T.; Tao, L.; Saur, G.; van 38 (5) de Lagemaat, J.; Kelley, S. O.; Sargent, E. H. What Should W61 39 Make with  $CO_2$  and How Can We Make It? Joule **2018**, 2 (502) 40 41 825-832. https://doi.org/10.1016/j.joule.2017.09.003. 103 Kumagai, H.; Nishikawa, T.; Koizumi, H.; Yatsu, T.; Sahara, 104 42 (6) 43 Yamazaki, Y.; Tamaki, Y.; Ishitani, O. Electrocatalytic Reduction of Low Concentration CO<sub>2</sub>. Chem. Sci. **2019**, 10 106 44 45 1597-1606. https://doi.org/10.1039/C8SC04124E. 107 46 (7) Kaminsky, C. J.; Wright, J.; Surendranath, Y. Graphite-Conjugation Enhances Porphyrin Electrocatalysis. ACS Catal 109 47 48 2019, 3667-3671. 110 49 https://doi.org/10.1021/acscatal.9b00404. Sampson, M. D.; Kubiak, C. P. Manganese Electrocatalysts 112 50 (8) 51 with Bulky Bipyridine Ligands: Utilizing Lewis Acids To Promote Carbon Dioxide Reduction at Low Overpotentials. J. 52

- Am. Chem. Soc. **2016**, 138 (4), 1386–1393. https://doi.org/10.1021/jacs.5b12215.
- (9) Takeda, H.; Ohashi, K.; Sekine, A.; Ishitani, O. Photocatalytic CO₂ Reduction Using Cu(I) Photosensitizers with a Fe(II) Catalyst. J. Am. Chem. Soc. 2016, 138 (13), 4354–4357. https://doi.org/10.1021/jacs.6b01970.
- (10) Froehlich, J. D.; Kubiak, C. P. The Homogeneous Reduction of CO<sub>2</sub> by [Ni(Cyclam)]\*: Increased Catalytic Rates with the Addition of a CO Scavenger. J. Am. Chem. Soc. 2015, 137 (10), 3565–3573. https://doi.org/10.1021/ja512575v.
- (11) Machan, C. W.; Stanton, C. J.; Vandezande, J. E.; Majetich, G. F.; Schaefer, H. F.; Kubiak, C. P.; Agarwal, J. Electrocatalytic Reduction of Carbon Dioxide by Mn(CN)(2,2'-Bipyridine)(CO)<sub>3</sub>: CN Coordination Alters Mechanism. *Inorg. Chem.* 2015, 54 (17), 8849–8856. https://doi.org/10.1021/acs.inorgchem.5b01715.
- (12) Agarwal, J.; Iii, C. J. S.; Shaw, T. W.; Vandezande, J. E.; Majetich, G. F.; Bocarsly, A. B.; Iii, H. F. S. Exploring the Effect of Axial Ligand Substitution (X = Br, NCS, CN) on the Photodecomposition and Electrochemical Activity of [MnX(N−C)(CO)₃] Complexes. *Dalton Trans.* **2015**, *44* (5), 2122–2131. https://doi.org/10.1039/C4DT03079F.
- (13) Bourrez, M.; Molton, F.; Chardon-Noblat, S.; Deronzier, A. [Mn(Bipyridyl)(CO)<sub>3</sub>Br]: An Abundant Metal Carbonyl Complex as Efficient Electrocatalyst for CO<sub>2</sub> Reduction. *Angew. Chem. Int. Ed.* **2011**, *50* (42), 9903–9906. https://doi.org/10.1002/anie.201103616.
- (14) Grills, D. C.; Ertem, M. Z.; McKinnon, M.; Ngo, K. T.; Rochford, J. Mechanistic Aspects of CO₂ Reduction Catalysis with Manganese-Based Molecular Catalysts. *Coord. Chem. Rev.* 2018, 374, 173–217. https://doi.org/10.1016/j.ccr.2018.05.022.
- (15) Smieja, J. M.; Sampson, M. D.; Grice, K. A.; Benson, E. E.; Froehlich, J. D.; Kubiak, C. P. Manganese as a Substitute for Rhenium in CO₂ Reduction Catalysts: The Importance of Acids. *Inorg. Chem.* 2013, 52 (5), 2484–2491. https://doi.org/10.1021/ic302391u.
- (17) Franco, F.; Pinto, M. F.; Royo, B.; Lloret-Fillol, J. A Highly Active N-Heterocyclic Carbene Manganese(I) Complex for Selective Electrocatalytic CO₂ Reduction to CO. Angew. Chem. Int. Ed. 2018, 57 (17), 4603–4606. https://doi.org/10.1002/anie.201800705.
- (18) Myren, T. H. T.; Lilio, A. M.; Huntzinger, C. G.; Horstman, J. W.; Stinson, T. A.; Donadt, T. B.; Moore, C.; Lama, B.; Funke, H. H.; Luca, O. R. Manganese N-Heterocyclic Carbene Pincers for the Electrocatalytic Reduction of Carbon Dioxide. *Organometallics* 2019, 38 (6), 1248–1253. https://doi.org/10.1021/acs.organomet.8b00535.
- (19) Stanton, C. J.; Vandezande, J. E.; Majetich, G. F.; Schaefer, H. F.; Agarwal, J. Mn-NHC Electrocatalysts: Increasing  $\pi$  Acidity Lowers the Reduction Potential and Increases the Turnover Frequency for  $CO_2$  Reduction. *Inorg. Chem.* **2016**, *55* (19), 9509–9512.
  - https://doi.org/10.1021/acs.inorgchem.6b01657.
- (20) Agarwal, J.; Shaw, T. W.; Stanton, C. J.; Majetich, G. F.; Bocarsly, A. B.; Schaefer, H. F. NHC-Containing Manganese(I) Electrocatalysts for the Two-Electron Reduction of CO<sub>2</sub>. Angew. Chem. Int. Ed. 2014, 53 (20), 5152–5155. https://doi.org/10.1002/anie.201311099.
- (21) Costentin, C.; Drouet, S.; Robert, M.; Savéant, J.-M. A Local Proton Source Enhances CO₂ Electroreduction to CO by a

ARTICLE Journal Name

- Molecular Fe Catalyst. Science 2012, 338 (6103), 90–94.
   https://doi.org/10.1126/science.1224581.
- 3 (22) Franco, F.; Cometto, C.; Nencini, L.; Barolo, C.; Sordello, F.;
  4 Minero, C.; Fiedler, J.; Robert, M.; Gobetto, R.; Nervi, C. Local
  5 Proton Source in Electrocatalytic CO<sub>2</sub> Reduction with
  6 [Mn(Bpy–R)(CO)<sub>3</sub>Br] Complexes. *Chem. Eur. J.* **2017**, *23*7 (20), 4782–4793. https://doi.org/10.1002/chem.201605546.
- 8 (23) Chapovetsky, A.; Welborn, M.; Luna, J. M.; Haiges, R.; Miller, 9 T. F.; Marinescu, S. C. Pendant Hydrogen-Bond Donors in Cobalt Catalysts Independently Enhance CO<sub>2</sub> Reduction. *ACS Cent. Sci.* **2018**, *4* (3), 397–404.
- 12 https://doi.org/10.1021/acscentsci.7b00607.
- 13 (24) Ngo, K. T.; McKinnon, M.; Mahanti, B.; Narayanan, R.; Grills,
   14 D. C.; Ertem, M. Z.; Rochford, J. Turning on the Protonation 15 First Pathway for Electrocatalytic CO<sub>2</sub> Reduction by
   16 Manganese Bipyridyl Tricarbonyl Complexes. J. Am. Chem.
   17 Soc. 2017, 139 (7), 2604–2618.
   18 https://doi.org/10.1021/jacs.6b08776.
- 19 (25) Agarwal, J.; Shaw, T. W.; Schaefer, H. F.; Bocarsly, A. B.
   20 Design of a Catalytic Active Site for Electrochemical CO<sub>2</sub>
   21 Reduction with Mn(I)-Tricarbonyl Species. *Inorg. Chem.* 2015,
   22 54 (11), 5285–5294.
- 23 https://doi.org/10.1021/acs.inorgchem.5b00233.
- Riplinger, C.; Sampson, M. D.; Ritzmann, A. M.; Kubiak, C. P.;
   Carter, E. A. Mechanistic Contrasts between Manganese and
   Rhenium Bipyridine Electrocatalysts for the Reduction of
   Carbon Dioxide. J. Am. Chem. Soc. 2014, 136 (46), 16285–
   16298. https://doi.org/10.1021/ja508192y.
- (27) Huheey, J. E. Inorganic Chemistry Principles of Structure and
   Reactivity (4th Edition)Hardcover, 4 edition.; Prentice Hall,
   1997.
- 32 (28) Anslyn, E. V.; Dougherty, D. A. *Modern Physical Organic Chemistry*; University Science Books, 2006.
- 34 (29) Advances in Physical Organic Chemistry, Volume 26 1st
   35 Edition https://www.elsevier.com/books/advances-in-physical-organic-chemistry/bethell/978-0-12-033526-8
   37 (accessed Apr 2, 2019).
   38